Surface effects in hyperspectral infrared measurements from the AIRS instrument on the Aqua satellite

Youri Plokhenko[1] and W. Paul Menzel[2]

[1] CIMSS, University of Wisconsin – Madison , 1225 W. Dayton St., Madison WI 53706
(608) 262 7287 , (608) 262-5974 (FAX) , YouriP@ssec.wisc.edu
[2] Office of Research and Applications, NOAA / NESDIS, 1225 W. Dayton St., Madison WI 53706

Abstract   Surface emissivity (SE) variations cause measurable changes in infrared radiances. To improve the accuracy of vertical temperature-moisture profiles retrieved from AIRS sounder infrared measurements, the surface emissivity must be accounted for in the solution of the inverse problem. The accuracy of atmospheric parameters retrieved depends on the measurement accuracy and accurate definition of measurement model. The associated inverse problem based upon the numerical solution of the radiative transfer equation (RTE) is ill posed. Disregarding the spectral-spatial variations of SE in the RTE magnifies the errors. Different types of surface cover, with different surface optical properties and extremely high spatial and temporal variations, restrict the use of a priori estimates of SE. The direct evaluation of SE is an effective alternative. The RTE solution includes the surface emissivity, the surface temperature, and the temperature-moisture profile. The RTE equation is solved using the method of least squares in coordinate descent based on the Gauss-Newton numerical schema. Results of SE estimation are demonstrated. The SE estimates over land show significant spectral-spatial variability. Accounting for the emissivity positively affects the atmospheric temperature-moisture profile estimates.

Introduction   To estimate the atmospheric temperature-humidity vertical distributions from the multi-spectral infrared measurements requires a numerical solution of the radiative transfer equation (RTE). Accounting for emissions from both the earth surface and the atmosphere is critical since even small SE variations cause measurable changes in the infrared radiances. The spectral-spatial variations of SE in RTE, if ignored, can drastically reduce the accuracy of the solution. An algorithm is described in Plokhenko and Menzel (2000 and 2003). Results of data analysis and experimental processing of AIRS nighttime spectral measurements from the granule 016 of September 6, 2002 are presented.

Data analysis and physical interpretation   The Atmospheric Infrared Sounder (AIRS) spectral channels along with their intended purposes are given in Aumann and Miller 1995. The measurements demonstrate the following properties: (a) surface reflection is substantially larger in shortwave (SW) bands than in longwave (LW) bands, (b) radiation absorption by cloud ice particles is substantially larger in LW than in SW bands, and (c) SW bands are less affected by variations of atmospheric moisture than LW bands. In processing the AIRS measurements, the solution of the inverse problem includes the surface emissivity, the surface temperature, and the vertical temperature-humidity profile. Only spectral measurements at cloud free pixels are processed. The RTE for the cloud free atmosphere is:

$$\tilde{J}^{\uparrow}(\theta) = \varepsilon_s(\theta)\tau^{\uparrow}(p_s,\theta)B[T_s] \; + \int\limits_{\tau^{\uparrow}(p_s,\theta)}^{1} B[T(p)] \; d\tau^{\uparrow}(p,\theta) + (1-\varepsilon(\theta))\tau^{\uparrow}(p_S,\theta) \int\limits_{1}^{\tau^{\uparrow}(p_s,\vartheta)} B[T(p)] \; d\tau^{\downarrow}(p,\vartheta) \; + \; \xi$$

where: $\tilde{J}^{\uparrow}(\theta)$ is the radiance measured at the angle of incidence θ; $\varepsilon_s(\theta)$ is the effective hemispherical directional SE at the angle θ; φ is the effective angle of incidence of the downwelling radiance; $\tau^{\uparrow}(p,\theta)$, $\tau^{\downarrow}(p,\vartheta)$ are the atmospheric upwelling and downwelling transmittances, $T(p)$ and $Q(p)$ are temperature and moisture profiles; T_s is the surface temperature; ξ is an error of the measurement. In the RTE, the optical surface effects are described by $\varepsilon_s(\theta), \; \vartheta$.

As a first guess of emissivity spectrum, the constant 0.94 is assumes. ECWMF forecasts of temperature-moisture profiles are used as a first guess (FG). The retrievals are successful if they improve upon the accuracy of the background FG. Because the FG is already quite good, there is the problem that model uncertainties are comparable to the amplitude of signal variations. An estimate of the emissivity spectrum is expected to reduce the measurement modeling uncertainties.

SE and vertical moisture-temperature profiles are estimated in parametric form. The emissivity spectrum variation is represented by 11 basis functions, the moisture vertical profile variation by 17 basis functions, the temperature vertical profile variation by 31 basis functions. The moisture basis functions are chosen so that they can describe both the solution and the underintegral kernel: the moisture profile is exponentially decreasing with altitude; the spectrum sensitivity to the moisture profile variation (functional derivative) is the exponentially increasing (in some sense) with altitude. Including the surface temperature estimate, a solution for 60 parameters is sought for (see Fig. 1). The non-linear Fredholm equation of the first kind is solved using a method of least squares in coordinate descent based on a Gauss-Newton numerical schema; 2378 channels are analyzed. Noisy measurements are rejected. Measurements in 2100 channels are used on average per retrieval at a pixel.
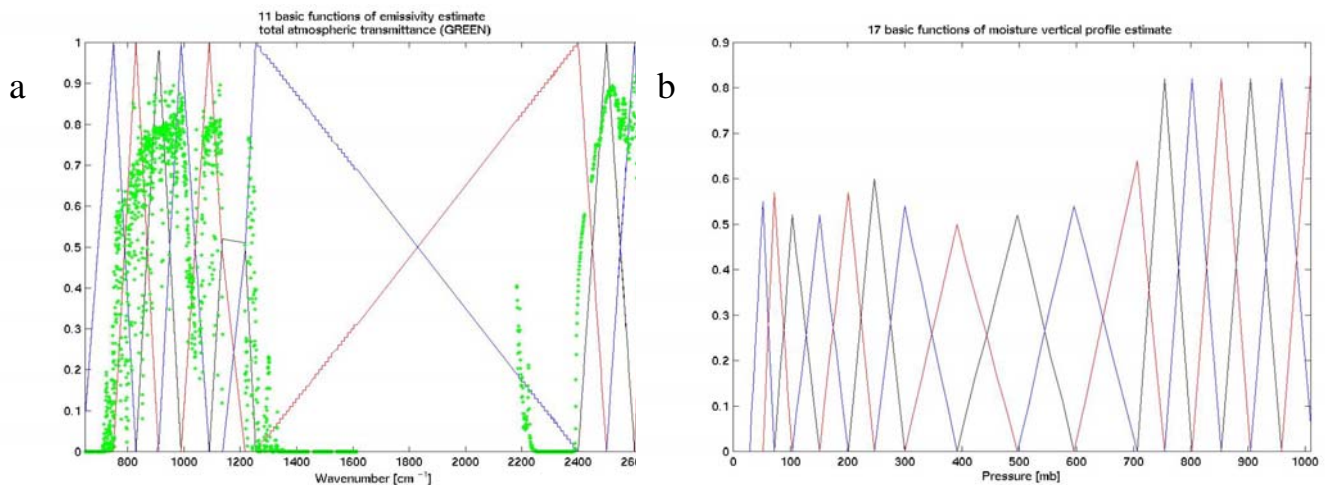

Figure 1. Solution components basis functions, (a) – emissivity spectrum (GREEN shows total atmospheric transmittance), (b) – atmospheric moisture.

Data analysis   The AIRS spectral measurements from the granule (total pixels number is 135 scan lines by 90 scan elements) 016 of September 6, 2002 are analyzed. It is nighttime data at 1h 40' GMT. The spectral information is stable, reliable and well calibrated. Surface elevation and meteorological conditions are shown in Figs 2(a,b,c,d). The spectral measurements cover a portion of Western Europe, Mediterranean Region and North Africa. Figure 2(a) shows complicated terrain, characterized by large variability of surface types (part of Sahara desert extreme right part of images) with significant differences in the surface optical properties. Figures 2(b,d) shows the spectral images [K] in SW (2555[1/cm]) and LW (944.1 [1/cm]) atmospheric windows, Fig.2(c) shows their spectral difference [K]. Areas in Fig 2(b,d) with low temperatures correspond to cloud atmosphere; areas with high temperatures correspond to the warm sea surface. There are distinctive differences in the spectral-spatial patterns corresponding to different surface types: small variability over water surface and noticeably larger over desert area. Fig 2(c) (spectral difference of the measurements from (b)– (d)) shows spectral peculiarities of atmospheric effects (related to clouds and water vapor areas) and surface optics effects (water surface and different types of land cover). Differences in the spectral absorption of cloud particles (size, phase) explain large spectral variability in the measurements: large positive differences correspond to high altitude clouds (low temperatures), negative differences occur for lower level clouds. Cloud free measurements over sea surface are characterized by high temperatures associated with the spatial-spectral uniformity (the small spectral variability of the reflection of the water surface). The measurement spatial

variability in LW window over water surface can be explained by the atmospheric water vapor absorption. The Mediterranean coastline of North Africa is clearly visible, indicating mostly cloud free atmospheric conditions at that region (some lower level clouds are visible at the upper right corner)
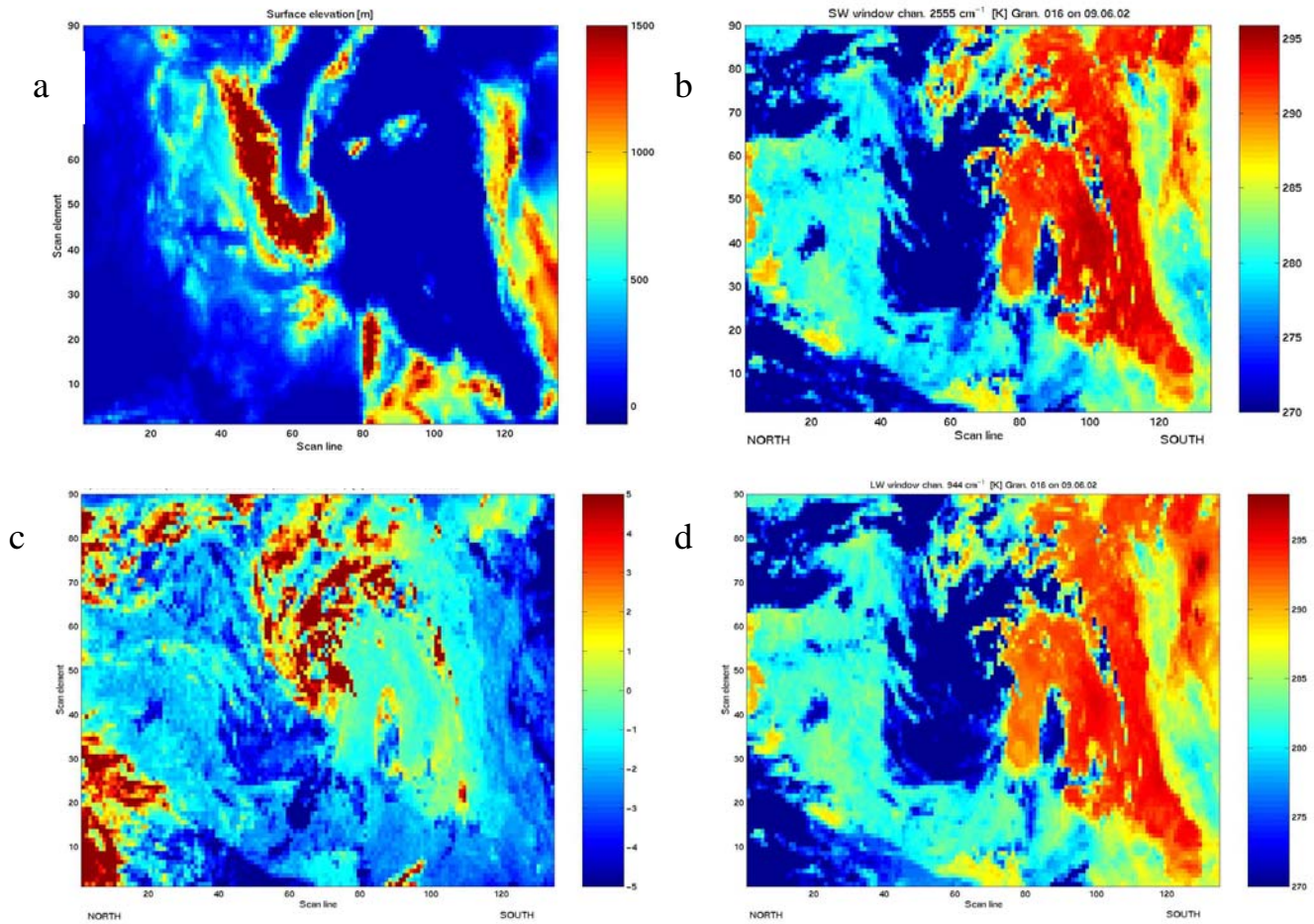

Figure 2 Surface elevation [m] (below 1500m) at sounding pixels (a); Spatial distribution of measurements [K] at atmospheric windows (b) 2555[1/cm] and (d) 944.1 [1/cm]; (c) spectral difference [K] of   measurements from (b – d)

The spatial-spectral analysis and spatial filtering of the measurements are effective tools in the meteorological analysis. It is important to reduce measurement uncertainties to reveal meteorologically meaningful signal. Spatial filtering reduces the influence of instrument noise. It is expected that the filtered measurements will have a nominal accuracy better than 0.2 K in all channels (see at Plokhenko and Menzel, 2001). Figures 3(a-d) show measurement error spectral distributions (a) and the effect of the spatial filtering in the lower stratospheric channel 7 at 651.05 1/cm (b,c,d). The spatial distribution of the original measurements in channel 7 (panel b) corresponds to measurement error 0.7 K, derived from onboard black body measurements. The spatial filter (averaging moving rectangular box) is 13 scan lines by 7 scan elements (for channel 7). Panel (c) shows measurement noise (difference (b) - (d)). The expected measurement error of filtered data from panel (c) is 0.07K. The improvement of signal to noise is significant.
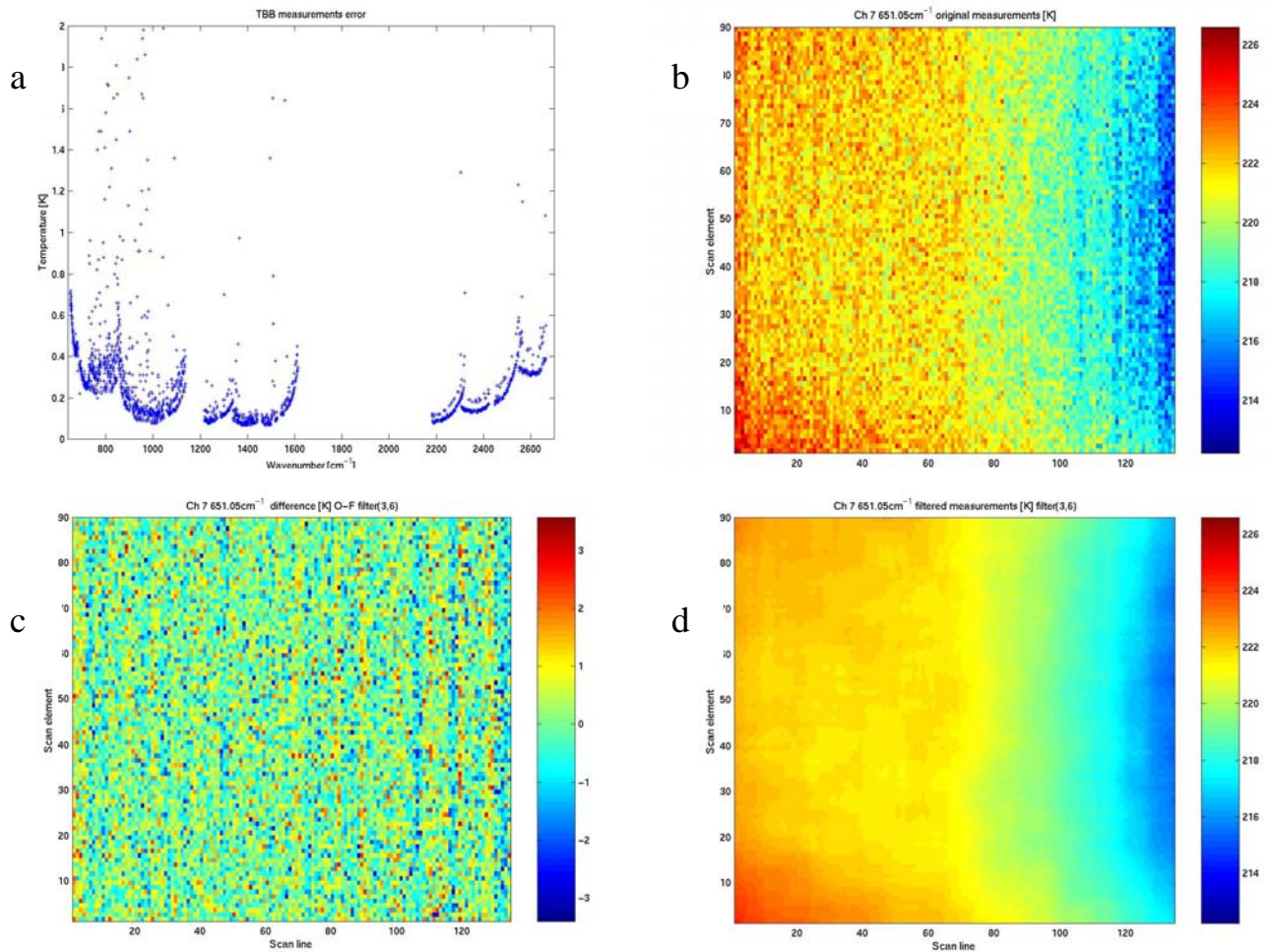
Figure 3 Measurements accuracy characteristics: (a) spectrum of standard deviation of measurement noise derived from black body measurements; (b,c,d) spatial distribution of measurements in channel 7 at 651.05 1/cm: (b) original measurements, (c) after spatial filtering, (d) difference (b-c).

 Results from Figs 3(a-d) show that spatial filtering significantly improves the measurements in upper tropospheric – lower stratospheric spectral channels. The spectral sensitivity to a variation +1K of the vertical temperature profile below 500hPa is shown in Fig 4(a). Panel (b) shows the spectral response to 0.02 increases in the surface emissivity (0.94 –0.96). Measurements in corresponding spectral channels are used for estimation surface of the emissivity spectrum and surface temperature.
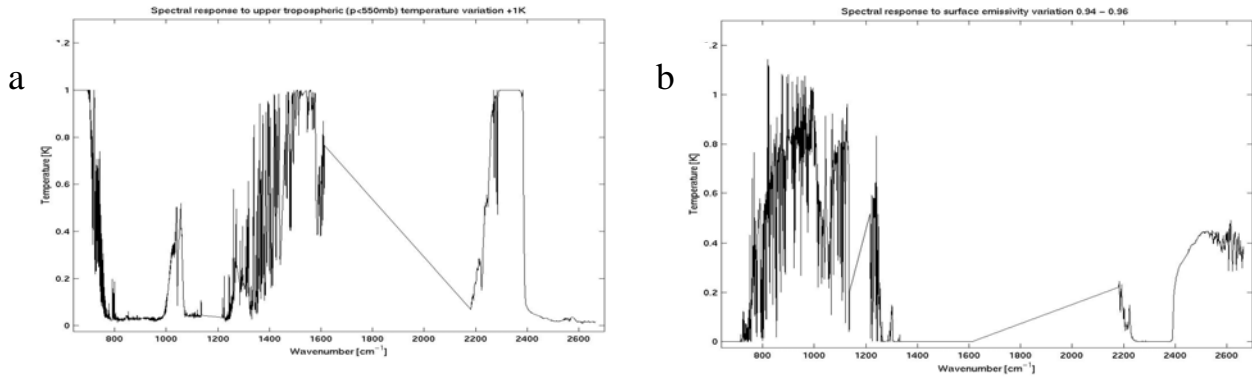
Figure 4(a,b) Measurements spectral characteristics: modeling measurements spectral response to: (a) - the 1K variation of the atmospheric temperature vertical profile below 500hPa and (b) – 0.02 variation of the surface emissivity (0.94 –0.96).

Expected spectral-spatial variability of the surface emissivity and its impact on modeling accuracy are shown in Figures 5(a,b). Panel (a) shows the laboratory measurements [%] of the sand surface reflection, it shows 25% variation. Panel (b) shows the radiance spectral response [%] to 2% emissivity variation.
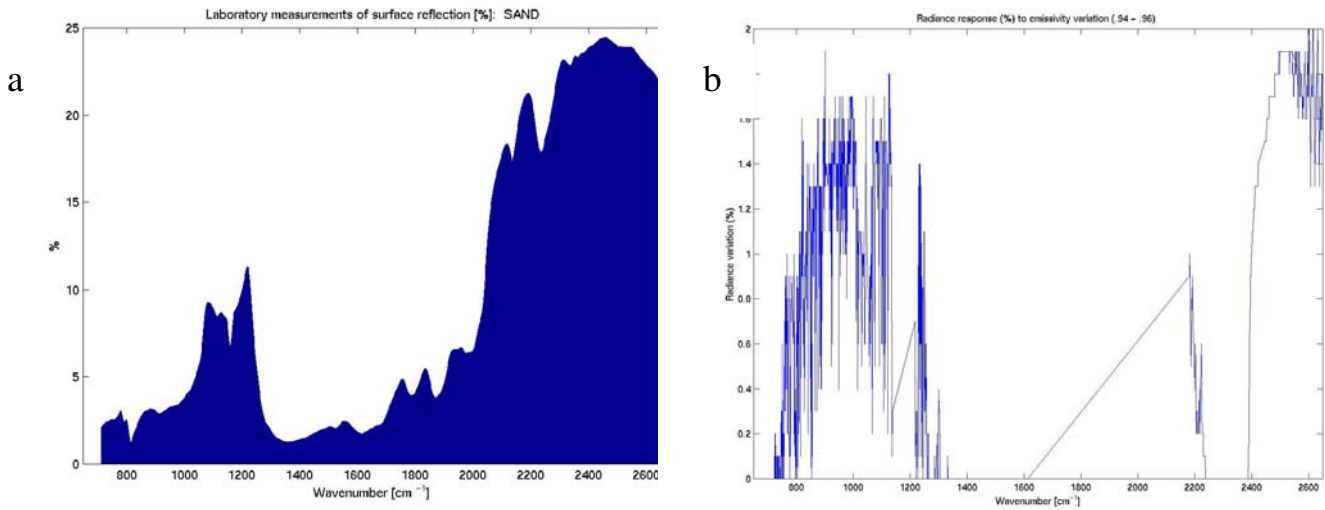

Figure 5 (a,b). The laboratory measurements [%] of the spectrum of the sand surface reflection (a); the radiance spectral response [%] to 2% emissivity variation

It follows from 5(a,b) that emissivity modeling error will substantially vary spatially and spectrally, especially affecting MW and SW measurements. Approximately 1% emissivity error will contribute 0.5% modeling error of measurement.

An example of spectral-spatial distribution of emissivity estimates derived from the AIRS nighttime measurements is shown in Fig 6(a-d). Figure 6a shows the spatial (latitudinal) crossection of emissivity estimates over North Africa (Sahara). It indicates two distinctive minima in the emissivity spectrum (compare with reflectivity in Fig 5a).
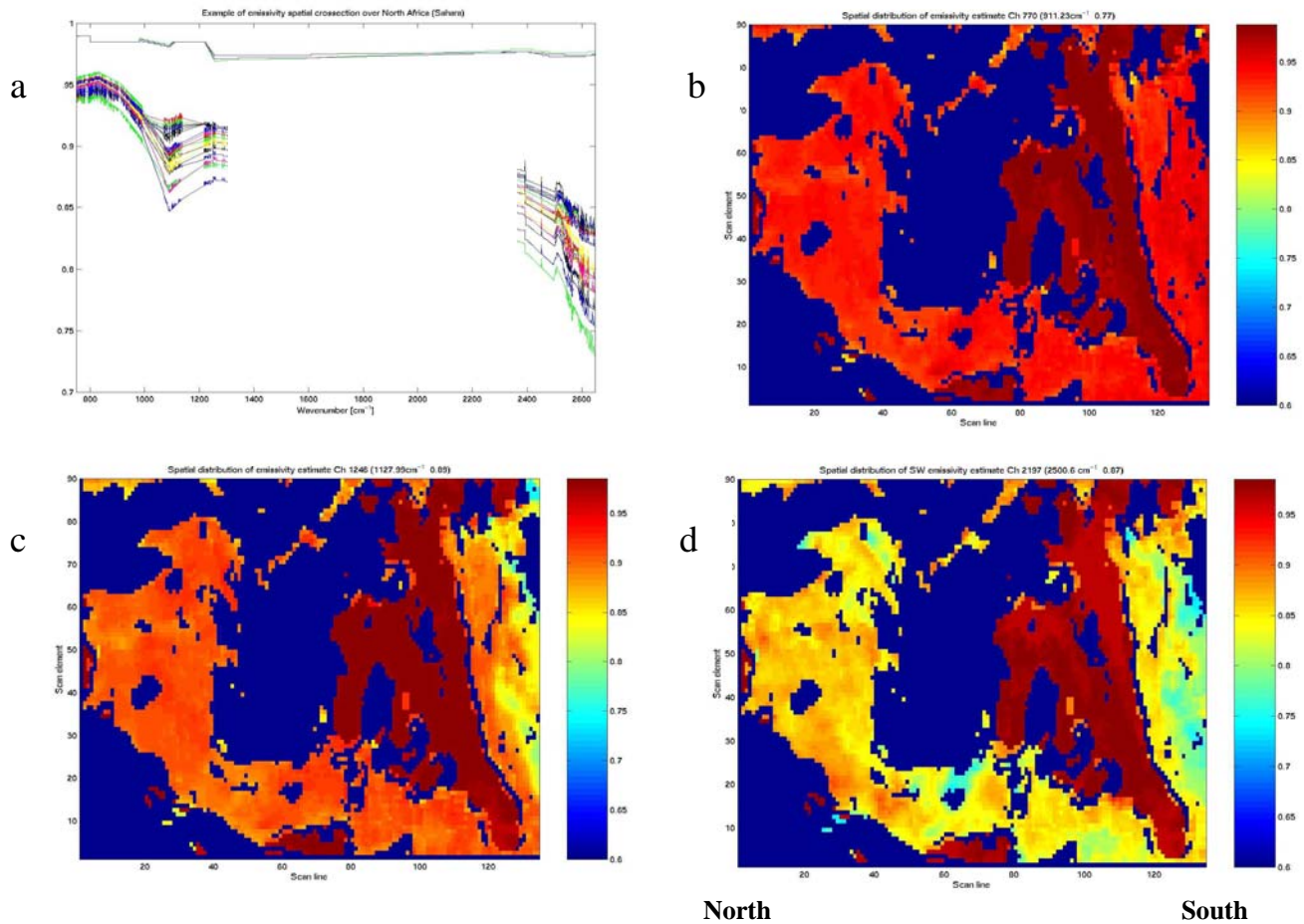
Figure 6 (a-d) Examples of spectral-spatial distributions of the emissivity estimates: (a) example of spatial (latitudinal) crossection of emissivity estimates over North Africa (Sahara); spatial distribution of emissivity estimates in Ch 977 at 990.34 [1/cm] (b), Ch 1246 at 1127.99 [1/cm] (c), Ch 2197 at 2500.6 [1/cm] (d) (dark blue areas correspond to missing data: clouds or solution low convergence at pixel). Dark red (high emissivity values) areas indicates water surface: Mediterranean Sea and North Africa shoreline are visible at the right parts of images. Sahara desert area is characterized by low emissivity at 9 and 4 μ bands.

The emissivity estimates vary from 0.7 to 0.96. Figures 6(b-d) show spatial distribution of the emissivity estimates at 11, 9 and 4μ. They show significant differences in spectral patterns of different surface types: there are distinctive differences between spatial-spectral patterns of Europe and North Africa. European areas are quite smooth (some variations relate to mount areas and cloud identification errors). North African areas vary at a noticeably larger scale.

Figures 7(a-f) demonstrate the spatial distribution and variability of the lower tropospheric moisture estimate at the pressure levels 950, 900 and 850hPa (figures 7(a-b)); the first guess fields are presented in figures 7(d-f) (units [%] in the data transformation $W_{s,f}(p)=100*(w_{s,f}(p)-\bar{w}_f(p))/\bar{w}_f(p)$, where mixing ratio profiles [g/kg] $w_{s,f}(p)$, $\bar{w}_f(p)$ (s-solution, f – first guess), the letter is average moisture profile for granule). Fig 7 (a-c) show solution fields at the cloud free pixels (see Figs. 6(b-d), FG is shown at cloud pixels). Figures 7(a-f) show that moisture
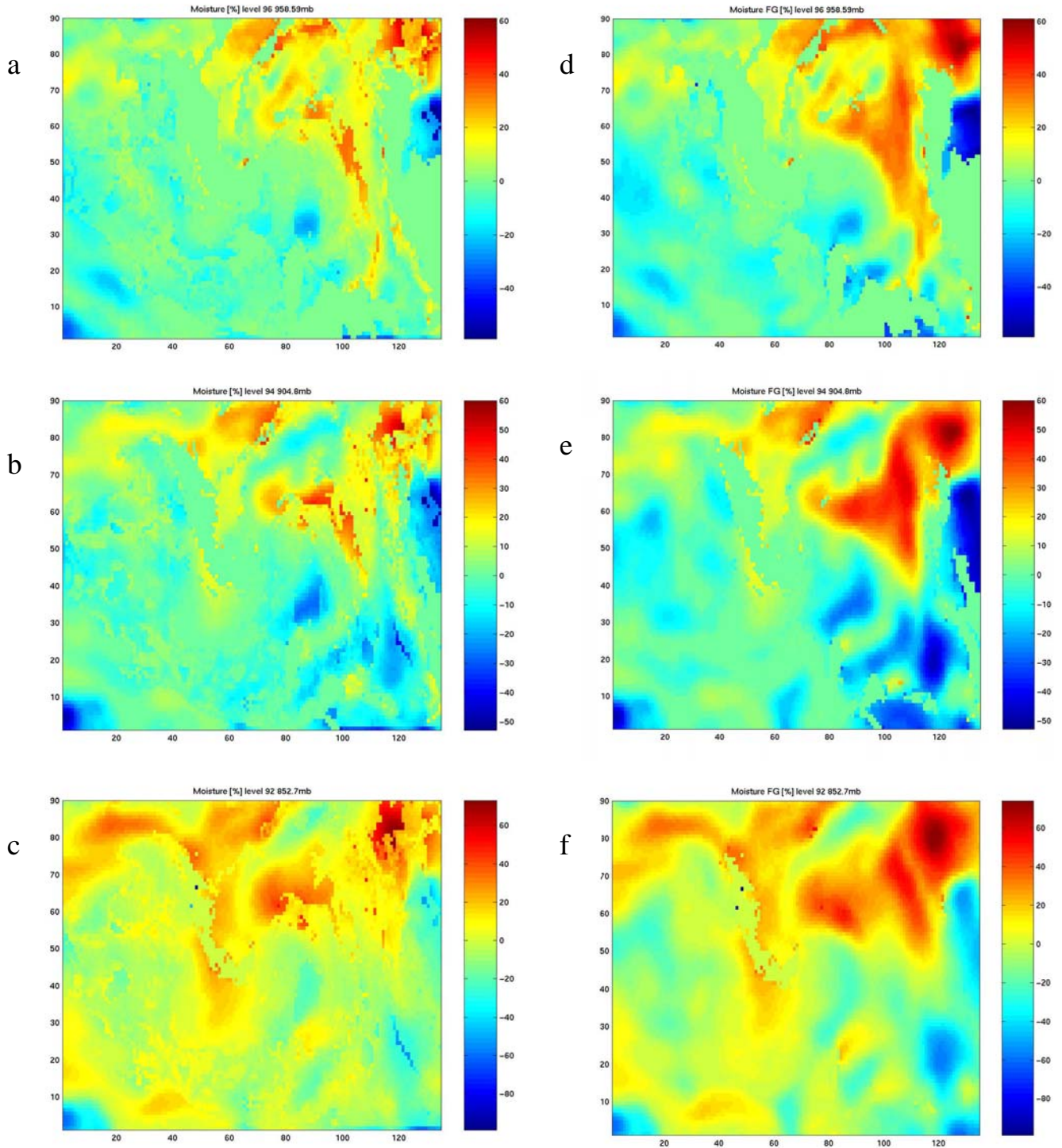
Figures 7 (a-f). The spatial distribution of the lower tropospheric moisture estimate at the pressure levels 950, 900 and 850mb: (a-b) –estimate [%], (d-f) – first guess [%] (from the ECMWF forecast) (units [%] in the data transformation $W_{s,f}(p)=100*(w_{s,f}(p)-\bar{w}_f(p))/\bar{w}_f(p)$, where mixing ratio profiles [g/kg] $w_{s,f}(p)$, $\bar{w}_f(p)$ (s-solution, f – first guess), the letter is average moisture profile for granule). The solution fields were imposed on the corresponding first guess fields from the (d-f) at the cloud free pixels (see Figs. 6(b-d))

Estimates in the lower troposphere are successfully retrieved from spectral measurements using non-linear model that includes the surface emissivity in the inverse problem solution. The solution is spatially consistent, major first guess spatial peculiarities are reshaped. The solution is retrieving new spatial features and noticeably modifying some dry / wet air pools. The solution amplitude is significant to 40%.

Conclusion Analysis of nighttime hyperspectral measurements from the AIRS instrument shows that SE significantly affects the infrared measurements. The spectral-spatial SE distributions at the AIRS spectral bands were estimated for the data from the granule 016 of September 6, 2002. An algorithm for solving the non-linear inverse problem to retrieve effective SE and temperature plus atmospheric moisture-temperature profiles was developed. Results show a strong spatial-spectral dependence in the surface variability. The spatial distribution of the SE estimates is coherent with the ecosystem characteristics. Direct evaluation of the SE in the inverse solution of the radiative transfer equation is an effective approach for accounting for surface optics. The vertical-spatial distributions of the estimates of atmospheric temperature and moisture are more components of the solutions.

References

Aumann, H.H., and Miller, Chris, "Atmospheric Infrared Sounder (AIRS) on the Earth Observing System", SPIE Vol.2583, 32-343, 1995.

Plokhenko, Y. and W. P. Menzel, 2000: The effects of surface reflection on estimating the vertical temperature-humidity distribution from spectral infrared measurements. Jour Appl. Meteor. **39**, 3-14.

Plokhenko, Y. and W. P. Menzel, 2001: Mathematical aspects in meteorological processing of infrared spectral measurements from the GOES sounder. Part I: Constructing the measurement estimates using spatial smoothing. Jour. Appl. Meteor, **40**, 556-567.

Plokhenko, Youri; Menzel; Bayler, Gail and Schmit, Timothy J. Mathematical Aspects in Meteorological Processing of Infrared Spectral Measurements from the GOES Sounder. Part II: Analysis of Spatial and Temporal Continuity of Spectral Measurements from the GOES-8 Sounder. Journal of Applied Meteorology: Vol. 42, No. 6, 2003, pp. 671–685.

Plokhenko, Youri and Menzel, W. Paul. Mathematical Aspects of the Meteorological Processing of Infrared Spectral Measurements from the GOES Sounder. Part III: Emissivity Estimation in Solving the Inverse Problem of Atmospheric Remote Sensing. Journal of Applied Meteorology: Vol. 42, No. 11, 2003, pp.1533-1546.

Proceedings
of the
Thirteenth International
TOVS Study Conference
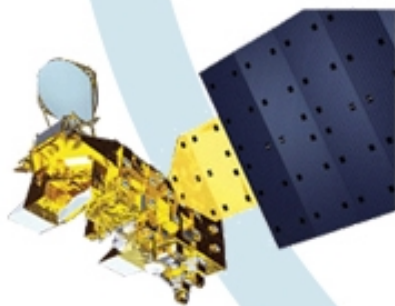
Sainte-Adèle, Québec, Canada
29 October – 4 November 2003